Title: Shared requirement for MYC upstream super-enhancer in tissue regeneration and cancer

Authors: Inderpreet Kaur Sur[1], Wenshuo Zhao[1], Jilin Zhang[1], Margareta Kling Pilström[1], Björn Rozell[9], Anna T. Webb[2], Huaitao Cheng[3], Ari Ristimäki[5,6], Pekka Katajisto[2,7,8], Martin Enge[3], Helena Rannikmae[4§], Marc de la Roche[4], Jussi Taipale[1,4,5] ✉

Affiliations:

[1]Department of Medical Biochemistry and Biophysics, Karolinska Institutet, Sweden.

[2]Department of Cell and Molecular Biology, Karolinska Institutet, Sweden.

[3]Department of Oncology and Pathology, Karolinska Institutet, Sweden.

[4]Department of Biochemistry, University of Cambridge, United Kingdom.

[5]Applied Tumor Genomics Program, University of Helsinki, Biomedicum, P.O. Box 63 (Haartmaninkatu 8), FIN-00014 University of Helsinki, Finland.

[6]Department of Pathology, HUSLAB, HUS Diagnostic Center, Helsinki University Hospital and University of Helsinki, Finland.

[7]Institute of Biotechnology, HiLIFE, University of Helsinki, Finland.

[8]Molecular and Integrative Bioscience Research Programme, Faculty of Biological and Environmental Sciences, University of Helsinki, Finland.

[9]Department of Laboratory Medicine, Karolinska Institutet, Sweden.

✉Corresponding Author: jussi.taipale@ki.se

[§]Present address: Complex In Vitro Models, In vitro/In Vivo Translation, GlaxoSmithKline, United Kingdom.

Abstract

Cancer has been characterized as a wound that does not heal. Malignant cells are morphologically distinct from normal proliferating cells, but have extensive similarities to tissues undergoing wound healing and/or regeneration. The mechanistic basis of this similarity has, however, remained enigmatic. Here we show that the genomic region upstream of Myc, which is required for intestinal tumorigenesis, is also required for intestinal regeneration after radiation damage. The region is also critical for growth of adult intestinal cells in 3D organoid culture, indicating that culture conditions that recapitulate most aspects of normal tissue architecture still reprogram normal cells to proliferate using a mechanism similar to that employed by cancer cells. Our results uncover a genetic link between tissue regeneration and tumorigenesis, and establish that normal tissue renewal and regeneration of tissues after severe damage are mechanistically distinct.

Summary: Myc regulatory region links regeneration and cancer

Out of all genomic regions, the 500 kb region upstream of MYC carries the largest burden of population-level cancer susceptibility (*1, 2*). We have previously deleted regulatory sequences syntenic to this region in mice (*3*), and demonstrated that the mice are healthy and fertile, yet resistant to intestinal and mammary tumors. Although deletion of the region did not cause major effect on fitness in our assays, the enhancer elements within this region are highly conserved between mammalian species (*4-10*). This suggests that the region would also have a beneficial biological function that would balance the negative impact of increased cancer predisposition.

To identify the biological role of the element, we first characterized the cellular architecture and expression profile of cells from the small intestine of the $Myc^{\Delta 2\text{-}540/\Delta 2\text{-}540}$ mice. We probed the intestinal crypt-villus axis of the mice for markers of stem cells, transit amplifying cells and major differentiated cell types. No difference in marker expression was observed between $Myc^{\Delta 2\text{-}540/\Delta 2\text{-}540}$ and wild-type mice (**Fig. 1A**). Furthermore, proliferation rates of intestinal cells appeared similar based on Ki67 staining (**Fig. 1A**). To further characterize the cell types and their gene expression patterns, we subjected intestinal cells from $Myc^{\Delta 2\text{-}540/\Delta 2\text{-}540}$ and wild-type mice to single-cell RNA sequencing (scRNA-seq). The cell type distributions and expression profiles were similar between the mice (**Fig. 1B**, fig. S1), except for almost complete lack of MYC expression from stem and transit amplifying cells of the $Myc^{\Delta 2\text{-}540/\Delta 2\text{-}540}$ mice (**Fig. 1C**). Consistently with this, single-cell ATAC-seq revealed that there were no compensatory changes in accessibility of MYC enhancer elements in $Myc^{\Delta 2\text{-}540/\Delta 2\text{-}540}$ mice (**Fig. 1D)**. Previously, we reported that although MYC was downregulated in the colon and small intestine of $Myc^{\Delta 2\text{-}540/\Delta 2\text{-}540}$ mice, most of the known MYC targets were not downregulated significantly in these tissues based on bulk RNA-seq (*3*). To determine whether MYC targets are induced in relatively rare cell types that express high levels of MYC in the intestine, we specifically analyzed expression of a set of 126 functionally conserved MYC targets from Zielke et al. (*11*), most of which are involved in metabolism and ribosome biogenesis. The regulation of this set of genes is conserved between *Drosophila* and humans. Analysis of expression of this gene set in stem cell and transit amplifying cell populations, which express MYC in wild-type mice, revealed that the functionally conserved MYC targets were modestly downregulated in $Myc^{\Delta 2\text{-}540/\Delta 2\text{-}540}$ mice (**Fig. 1C**, table S1). By contrast, there was no downregulation of the set of genes in mature enterocytes, which do not express MYC. These results establish that normal intestinal morphogenesis and proliferation are essentially unperturbed in $Myc^{\Delta 2\text{-}540/\Delta 2\text{-}540}$ mice, despite dramatic downregulation of MYC. We observed an increase in L-

MYC expression within the stem cell and transit amplifying cell clusters of *Myc*$^{\Delta 2\text{-}540/\Delta 2\text{-}540}$ mice (fig. S2) suggesting compensation of MYC function during normal homeostasis. Taken together the results suggest that MYC may only be required during intestinal development (*12, 13*) and during proliferation associated with pathological condition (*3*).

We have earlier shown that *Myc*$^{\Delta 2\text{-}540/\Delta 2\text{-}540}$ mice and mice deficient of a single enhancer at the MYC locus (*Myc-335*$^{-/-}$) display 98% and 70% resistance to intestinal polyps on APC^{Min} background. Nevertheless, both types of mice do develop polyps, and we reasoned that characterizing the polyps from *Apc*$^{Min/+}$*; Myc-335*$^{-/-}$ and *Apc*$^{Min/+}$*; Myc*$^{\Delta 2\text{-}540/\Delta 2\text{-}540}$ mice would help us to understand the role of MYC and its enhancer elements in tumorigenesis. We first measured disease-free survival of *Apc*$^{Min/+}$ mice on wild-type, *Myc-335*$^{-/-}$ and *Myc*$^{\Delta 2\text{-}540/\Delta 2\text{-}540}$ backgrounds. This analysis confirmed and extended our earlier findings (*3, 14*) that the MYC enhancer deficient mice are resistant to tumorigenesis. *Myc-335*$^{-/-}$ mice survived longer than wild-type mice, but eventually had to be sacrificed by 1 year of age due to intestinal polyposis (Median survival=306 days [n=7] compared to 156 days for *Apc*$^{Min/+}$ [n=9]). In contrast, all four studied *Myc*$^{\Delta 2\text{-}540/\Delta 2\text{-}540}$ lived without observable adverse health effects for more than 500 days, but developed symptoms consistent with intestinal tumorigenesis prior to two years of age. The median survival was 584 days (19.5 months), corresponding to normal old age in C57BL/6 strain (18-24 months) (*15*) (**Fig. 2A**).

Analysis of the polyp size from four month old *Apc*$^{Min/+}$, *Apc*$^{Min/+}$*;Myc-335*$^{-/-}$ and *Apc*$^{Min/+}$*;Myc*$^{\Delta 2\text{-}540/\Delta 2\text{-}540}$ mice revealed that although the number of polyps was very different, the sizes of the polyps were similar between all the backgrounds (**Fig. 2B**). Morphological analysis of the polyps from the *Apc*$^{Min/+}$*;Myc-335*$^{-/-}$ mice did not reveal any differences from the polyps found in *Apc*$^{Min/+}$ mice, but some of the polyps from the *Apc*$^{Min/+}$*;Myc*$^{\Delta 2\text{-}540/\Delta 2\text{-}540}$ mice appeared flatter and more dense in morphology compared to the *Apc*$^{Min/+}$ polyps (**Fig. 2C**,**D**). Notably, two out of four more than one year old *Apc*$^{Min/+}$*;Myc*$^{\Delta 2\text{-}540/\Delta 2\text{-}540}$ mice that we analysed had developed larger, non-polypoid small intestinal tumors with a morphology that was very distinct from that of the polypoid tumors (**Fig. 2D**,**E)**. These tumors appeared to have a 'pushing edge' growth pattern instead of the finger-like pattern common to polyps. A female, old *Apc*$^{Min/+}$*;Myc*$^{\Delta 2\text{-}540/\Delta 2\text{-}540}$ mouse also developed squamous cell metaplasia in the mammary gland (**Fig. 2F**). These results establish that the MYC upstream super-enhancer is necessary for formation of a particular common type of intestinal tumors, but does not completely eliminate tumorigenesis in the intestine.

The apparently specific role of the 2-540 kb conserved region in tumorigenesis is enigmatic, as a tumor-predisposing region would be expected to have a negative impact on fitness. We therefore hypothesized that the 2-540 kb region would be beneficial under some environmental condition that the mice fed well and housed in a relatively clean laboratory environment would not encounter. To test this, we subjected the $Myc^{\Delta 2\text{-}540/\Delta 2\text{-}540}$ mice to ionizing radiation, which induces a uniform and highly reproducible damage to the intestinal lining (*16, 17*). Wild-type mice gamma irradiated for a total dose of 12 Grays rapidly developed intestinal damage and lost 7.0 ± 0.8% of their weight in 3 days (n=19); the weight loss stabilized at that time, and the damage was largely repaired by day 5. By contrast, the $Myc^{\Delta 2\text{-}540/\Delta 2\text{-}540}$ mice appeared unable to repair the damage, as they continued to lose weight beyond 3 days, losing on average 17% by 5 days (n=10) (**Fig. 3A**,**B**). Morphological analysis of the small intestines confirmed that the damage was repaired in the wild-type mice but, sustained in the $Myc^{\Delta 2\text{-}540/\Delta 2\text{-}540}$ mice due to failure to regenerate the intestinal crypts (**Fig. 3C**). The wild-type mice displayed robust MYC induction at 3 days, and a strong proliferative response at 5 days, whereas at the same time points, in the $Myc^{\Delta 2\text{-}540/\Delta 2\text{-}540}$ mice MYC expression was undetectable and there was almost complete absence of proliferating cells (**Fig. 3D-F**, fig. S3). Single-cell RNA-seq analysis at day 2 revealed that the MYC expression was limited to stem and transit amplifying cells of wild-type mice. Despite the tissue damage, stem cells or transit amplifying cells from irradiated $Myc^{\Delta 2\text{-}540/\Delta 2\text{-}540}$ mice expressed almost no MYC, the signal being even lower than that from irradiated mature enterocytes of wild-type mice (**Fig. 3G**). Consistently with this result, unbiased gene set enrichment analysis revealed that a set of MYC targets (V1) failed to be upregulated by irradiation in stem cells of the $Myc^{\Delta 2\text{-}540/\Delta 2\text{-}540}$ mice (**Fig. 3H**, table S2). The functionally conserved MYC targets were also strongly upregulated in the stem-cells of irradiated wild-type mice compared to $Myc^{\Delta 2\text{-}540/\Delta 2\text{-}540}$ mice (**Fig. 3I**). These results establish that the 2-540 kb conserved region is required both for tumorigenesis, and for repair of intestinal lining after acute large-scale damage.

To further characterize the role of MYC in tissue repair, we decided to test a recently described model where intestine is decellularized and empty crypts are repopulated by cells derived from separate intestinal crypt preparations (*18*). Whereas cultures of wild-type crypts repopulated the decellularized intestinal scaffolds, crypts from $Myc^{\Delta 2\text{-}540/\Delta 2\text{-}540}$ mice failed to repopulate the scaffolds (**Fig. 4A**). As repopulation of the bare decellularized ECM requires cellular motility, with proliferation and self-renewal restricted to the empty crypt pits, we next placed isolated crypts in

standard organoid culture conditions in matrigel. Surprisingly, adult intestinal organoids from *Myc*$^{\Delta 2\text{-}540/\Delta 2\text{-}540}$ mice failed to grow also in such culture, where self-renewal and proliferation promoting signals are provided evenly (**Fig. 4B**). These results establish that although the Myc upstream super-enhancer region is not required for normal tissue renewal in mouse intestine, it is required for growth of adult intestinal cells under organoid culture conditions.

We show here that the same genetic element, the MYC upstream super-enhancer region, is required for both tissue renewal after radiation damage, and tumorigenesis. These results establish the long-sought mechanistic link between wound healing and cancer, and show that proliferation during normal homeostasis and tissue regeneration use regulatory mechanisms that are genetically distinct. Given that upregulation of ribosome biogenesis is required for Myc-driven proliferation (*11, 19, 20*), the simplest model consistent with our findings is that different levels of protein synthesis are needed for distinct proliferative cell fate choices. In this model, lower levels of protein synthesis and MYC are needed for proliferation that maintains stem cell number in tissue renewal, compared to processes that require exponential increase in the number of somatic stem cells, such as cell proliferation *in vitro,* regeneration, and tumorigenesis (**Fig. 4C**). Interestingly, the model has similarities to growth control in unicellular species, where nutrient availability specifies the protein synthetic rate and controls the balance between non-proliferative and proliferative states (*21*). Multicellularity could have evolved simply by the addition of a hierarchy of stem cells with new proliferative fates, which remain controlled by the same input variable, the total metabolic activity per genome. Consistently with this model, ES cells lacking MYC enter into a diapause-like non-proliferative state *in vitro* (*22*), and we also observe here that adult intestinal cells from *Myc*$^{\Delta 2\text{-}540/\Delta 2\text{-}540}$ mice enter a non-proliferative state under full mitogen stimulation (organoid culture).

Our results also show that cell culture models that are often considered to resemble normal *in vivo* tissue renewal actually drive cells to adopt an exponential cell proliferation program associated with regeneration and tumorigenesis. This has important consequences for drug development. In particular, compounds that inhibit proliferation of normal cells in culture have commonly been discarded during the development process due to toxicity, even when a subset of them may actually target the very mechanism that is distinct between normal proliferative cells and cancer cells.

REFERENCES

1. A. Buniello *et al.*, The NHGRI-EBI GWAS Catalog of published genome-wide association studies, targeted arrays and summary statistics 2019. *Nucleic Acids Res* **47**, D1005-D1012 (2019).
2. I. Sur, S. Tuupanen, T. Whitington, L. A. Aaltonen, J. Taipale, Lessons from functional analysis of genome-wide association studies. *Cancer Res* **73**, 4180-4184 (2013).
3. K. Dave *et al.*, Mice deficient of Myc super-enhancer region reveal differential control mechanism between normal and pathological growth. *Elife* **6**, (2017).
4. N. Ahmadiyeh *et al.*, 8q24 prostate, breast, and colon cancer risk loci show tissue-specific long-range interaction with MYC. *Proc Natl Acad Sci U S A* **107**, 9742-9746 (2010).
5. O. Hallikas *et al.*, Genome-wide prediction of mammalian enhancers based on analysis of transcription-factor binding affinity. *Cell* **124**, 47-59 (2006).
6. D. Hnisz *et al.*, Super-enhancers in the control of cell identity and disease. *Cell* **155**, 934-947 (2013).
7. M. M. Pomerantz *et al.*, The 8q24 cancer risk variant rs6983267 shows long-range interaction with MYC in colorectal cancer. *Nat Genet* **41**, 882-884 (2009).
8. J. Sotelo *et al.*, Long-range enhancers on 8q24 regulate c-Myc. *Proc Natl Acad Sci U S A* **107**, 3001-3005 (2010).
9. S. Tuupanen *et al.*, The common colorectal cancer predisposition SNP rs6983267 at chromosome 8q24 confers potential to enhanced Wnt signaling. *Nat Genet* **41**, 885-890 (2009).
10. J. Yan *et al.*, Transcription factor binding in human cells occurs in dense clusters formed around cohesin anchor sites. *Cell* **154**, 801-813 (2013).
11. N. Zielke, A. Vaharautio, J. Liu, T. Kivioja, J. Taipale, Upregulation of ribosome biogenesis via canonical E-boxes is required for Myc-driven proliferation. *Dev Cell* **57**, 1024-1036 e1025 (2022).
12. M. D. Bettess *et al.*, c-Myc is required for the formation of intestinal crypts but dispensable for homeostasis of the adult intestinal epithelium. *Mol Cell Biol* **25**, 7868-7878 (2005).
13. J. C. Cohen *et al.*, Transient in utero knockout (TIUKO) of C-MYC affects late lung and intestinal development in the mouse. *BMC Dev Biol* **4**, 4 (2004).
14. I. K. Sur *et al.*, Mice lacking a Myc enhancer that includes human SNP rs6983267 are resistant to intestinal tumors. *Science* **338**, 1360-1363 (2012).
15. J. G. Fox *et al.*, *The mouse in biomedical research: normative biology, husbandry, and models*. (Elsevier, 2006), vol. 3.
16. J. Gu *et al.*, At What Dose Can Total Body and Whole Abdominal Irradiation Cause Lethal Intestinal Injury Among C57BL/6J Mice? *Dose Response* **18**, 1559325820956783 (2020).
17. C. K. Kim, V. W. Yang, A. B. Bialkowska, The Role of Intestinal Stem Cells in Epithelial Regeneration Following Radiation-Induced Gut Injury. *Curr Stem Cell Rep* **3**, 320-332 (2017).
18. S. Iqbal *et al.*, Fetal-like reversion in the regenerating intestine is regulated by mesenchymal Asporin. *bioRxiv*, 2021.2006.2024.449590 (2021).
19. J. van Riggelen, A. Yetil, D. W. Felsher, MYC as a regulator of ribosome biogenesis and protein synthesis. *Nat Rev Cancer* **10**, 301-309 (2010).

20. P. Pihlajamaa, O. Kauko, B. Sahu, T. Kivioja, J. Taipale, A competitive precision CRISPR method to identify the fitness effects of transcription factor binding sites. *Nat Biotechnol*, (2022).
21. P. Jorgensen, M. Tyers, How cells coordinate growth and division. *Curr Biol* **14**, R1014-1027 (2004).
22. R. Scognamiglio *et al.*, Myc Depletion Induces a Pluripotent Dormant State Mimicking Diapause. *Cell* **164**, 668-680 (2016).
23. T. Sato, H. Clevers, Primary mouse small intestinal epithelial cell cultures. *Methods Mol Biol* **945**, 319-328 (2013).
24. F. A. Wolf, P. Angerer, F. J. Theis, SCANPY: large-scale single-cell gene expression data analysis. *Genome Biol* **19**, 15 (2018).
25. R. Lopez, J. Regier, M. B. Cole, M. I. Jordan, N. Yosef, Deep generative modeling for single-cell transcriptomics. *Nat Methods* **15**, 1053-1058 (2018).
26. M. K. Yum *et al.*, Tracing oncogene-driven remodelling of the intestinal stem cell niche. *Nature* **594**, 442-447 (2021).
27. A. T. Lun, K. Bach, J. C. Marioni, Pooling across cells to normalize single-cell RNA sequencing data with many zero counts. *Genome Biol* **17**, 75 (2016).
28. M. Ashburner *et al.*, Gene ontology: tool for the unification of biology. The Gene Ontology Consortium. *Nat Genet* **25**, 25-29 (2000).
29. A. Liberzon *et al.*, The Molecular Signatures Database (MSigDB) hallmark gene set collection. *Cell Syst* **1**, 417-425 (2015).
30. H. Cheng *et al.*, Smart3-ATAC: a highly sensitive method for joint accessibility and full-length transcriptome analysis in single cells. *bioRxiv*, 2021.2012.2002.470912 (2021).
31. N. Andrews *et al.*, An unsupervised method for physical cell interaction profiling of complex tissues. *Nat Methods* **18**, 912-920 (2021).
32. H. Li, R. Durbin, Fast and accurate long-read alignment with Burrows-Wheeler transform. *Bioinformatics* **26**, 589-595 (2010).
33. H. M. Amemiya, A. Kundaje, A. P. Boyle, The ENCODE Blacklist: Identification of Problematic Regions of the Genome. *Sci Rep* **9**, 9354 (2019).
34. K. Miyoshi *et al.*, Activation of beta -catenin signaling in differentiated mammary secretory cells induces transdifferentiation into epidermis and squamous metaplasias. *Proc Natl Acad Sci U S A* **99**, 219-224 (2002).

Acknowledgements

The authors wish to thank Drs Rong Yu, Yujiao Wu and Ekaterina Morgunova for their comments on the manuscript. We also wish to thank the core facilities at KI: The unit for morphological phenotype analysis (FENO) and the Bioinformatics and expression analysis core facility (BEA).

Funding: The study was supported by grants from the Swedish Research Council (D0815201) and Cancerfonden (20 1116 PjF 02H).

Author Contributions:

Conceptualization: IKS, JT
Investigation: IKS, WZ, JZ, MKP, BR, AW, HC, ME, AR, HR
Funding Acquisition: JT
Supervision: JT, IKS, PK, MR, JZ
Writing- original draft: JT, IKS
Writing- review & editing:IKS, WZ, JZ, MKP, BR, AW, HC, ME, AR, PK, HR, MR,JT

Data and materials availability: Sequencing data will be uploaded to European Nucleotide Archive (ENA, EMBL-EBI).

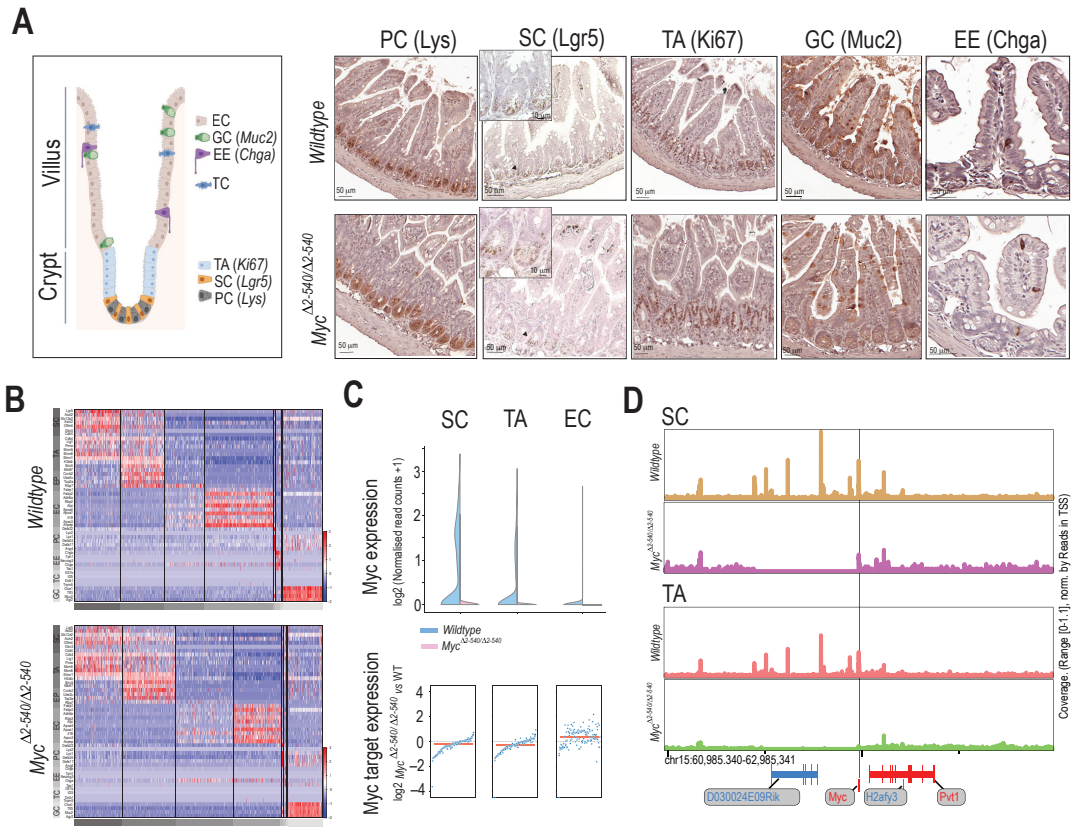

Fig. 1. *Myc*$^{\Delta 2\text{-}540/\Delta 2\text{-}540}$ intestine has a normal differentiation program during homeostasis (a) Similar pattern of cell-type specific marker expression in the wildtype and *Myc*$^{\Delta 2\text{-}540/\Delta 2\text{-}540}$ intestine. IHC staining for Lysozyme (Lys), Ki67, Mucin2 (Muc2), Chromogranin A (Chga) and ISH staining for Lgr5 are shown. Left most panel: schematic of different cell types present within the intestinal epithelium. (b) Heat map showing that all the major cell types of the intestine can be identified from single-cell RNA-seq analysis of intestinal crypts in both the wildtype and *Myc*$^{\Delta 2\text{-}540/\Delta 2\text{-}540}$ mice. Clustering was done using top 2000 highly variable genes and cell type specific markers were according to Yum *et al* (*26*). (c) single-cell RNA-seq confirmed dramatic reduction in Myc expression within the SC and TA clusters which resulted in a modest cell-type specific downregulation of Myc targets. Red line denotes the median expression of Myc targets. (d) single-cell ATAC-seq analysis showing absence of compensatory changes in accessibility of Myc enhancer elements around the 538 kb enhancer region deleted in *Myc*$^{\Delta 2\text{-}540/\Delta 2\text{-}540}$. PC: paneth cell, SC: stem cell; TA: transit amplifying cell, EE: enteroendocrine, TC: tuft cell; GC: goblet cell; EC: enterocyte; EP: enterocyte progenitor.

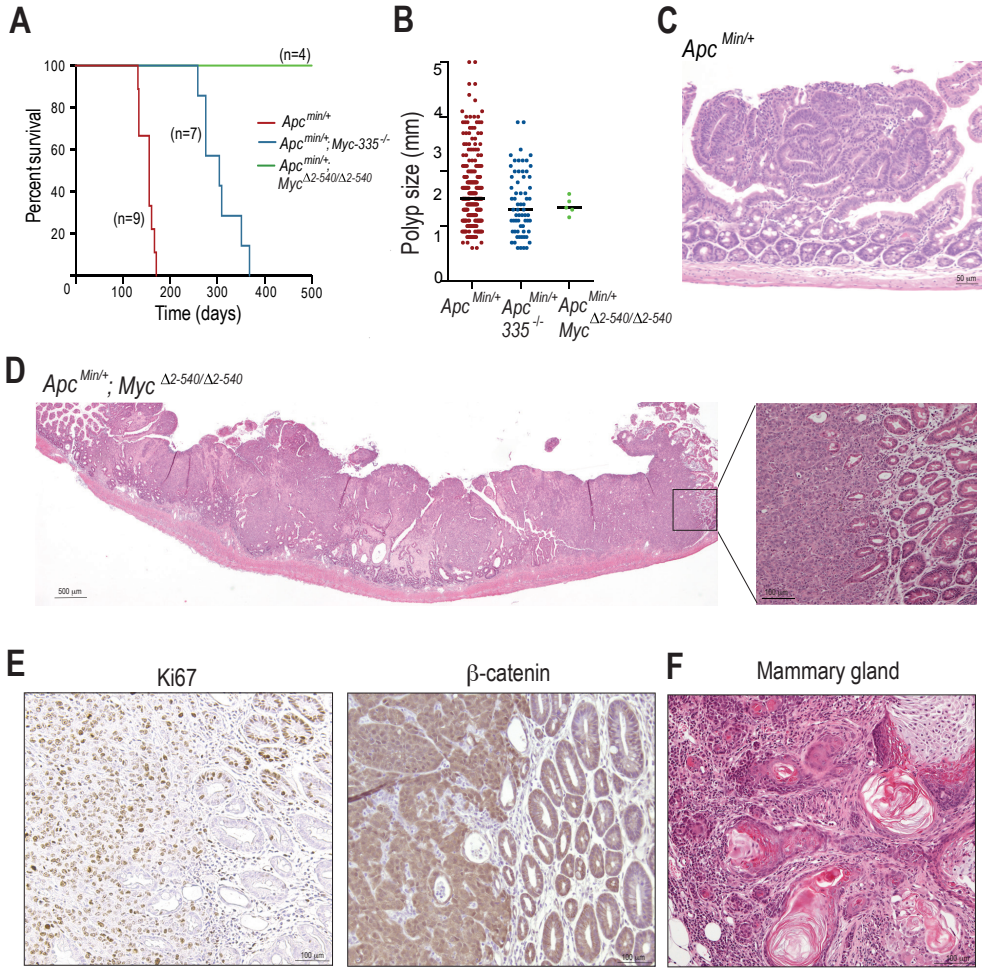

Fig. 2. Reduction in Myc impacts tumor initiation and spectrum (a) $Apc^{Min/+}$; $Myc^{\Delta 2\text{-}540/\Delta 2\text{-}540}$ survive to old age (average=19 months, n=4) compared to $Apc^{Min/+}$ (average=5 months, n=9). (b) There is no marked reduction in polyp size (diameter) at 4 months of age. (c-d) The polypoid nature of $Apc^{Min/+}$ tumors (c) is predominantly lost in the few tumors that develop in old $Apc^{Min/+}$; $Myc^{\Delta 2\text{-}540/\Delta 2\text{-}540}$ mice (d). A tumor from 1.5 years old $Apc^{Min/+}$; $Myc^{\Delta 2\text{-}540/\Delta 2\text{-}540}$ is shown. (e) IHC showing proliferation (Ki67) and active nuclear β-catenin within the tumor of old $Apc^{Min/+}$; $Myc^{\Delta 2\text{-}540/\Delta 2\text{-}540}$ mice. (f) HE stained section showing squamous cell metaplasia of mammary glands in old $Apc^{Min/+}$;$Myc^{\Delta 2\text{-}540/\Delta 2\text{-}540}$ mice. The observed metaplasia is consistent with a constitutive activation of β-catenin in the mammary gland (*34*).

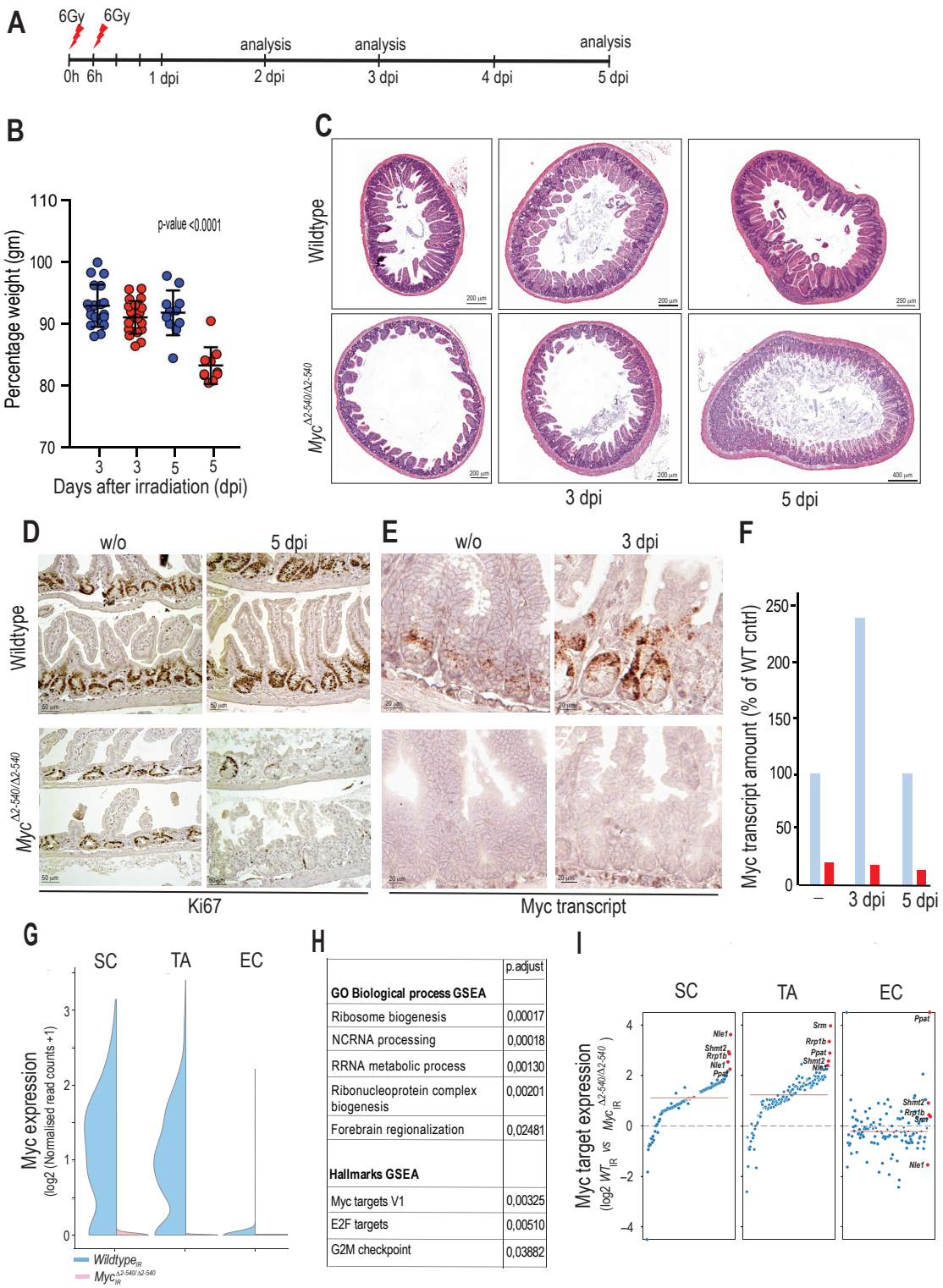

Fig. 3. *Myc*$^{\Delta 2\text{-}540/\Delta 2\text{-}540}$ intestine fails to support regenerative growth *in vivo* post γ-irradiation

(a) Timeline of the irradiation experiment. (b) *Myc*$^{\Delta 2\text{-}540/\Delta 2\text{-}540}$ mice (red) are more sensitive to weight loss post irradiation compared to wildtype mice (blue). (c) HE stained sections of small

intestine showing *Myc*$^{\Delta 2\text{-}540/\Delta 2\text{-}540}$ mice fail to regenerate crypts after radiation induced damage. (d) Failure to regenerate the crypts is associated with loss of proliferation as shown by IHC for proliferation marker Ki67. (e-g) Unlike the wildtype, *Myc*$^{\Delta 2\text{-}540/\Delta 2\text{-}540}$ intestine is unable to upregulate Myc expression after irradiation (e): ISH; (f): qPCR; (g): scRNA-seq (2 dpi). (h) GSEA analysis showing the most enriched gene ontology and hallmarks gene sets in the intestinal SC cluster of irradiated (2 dpi) wildtype mice compared to *Myc*$^{\Delta 2\text{-}540/\Delta 2\text{-}540}$ mice. (i) Irradiation results in strong induction of Myc targets in wildtype mice (2 dpi). Red line denotes the median expression of Myc targets. Red dots denote the top 5 differentially induced Myc targets in the stem cell compartment. dpi: days post irradiation.

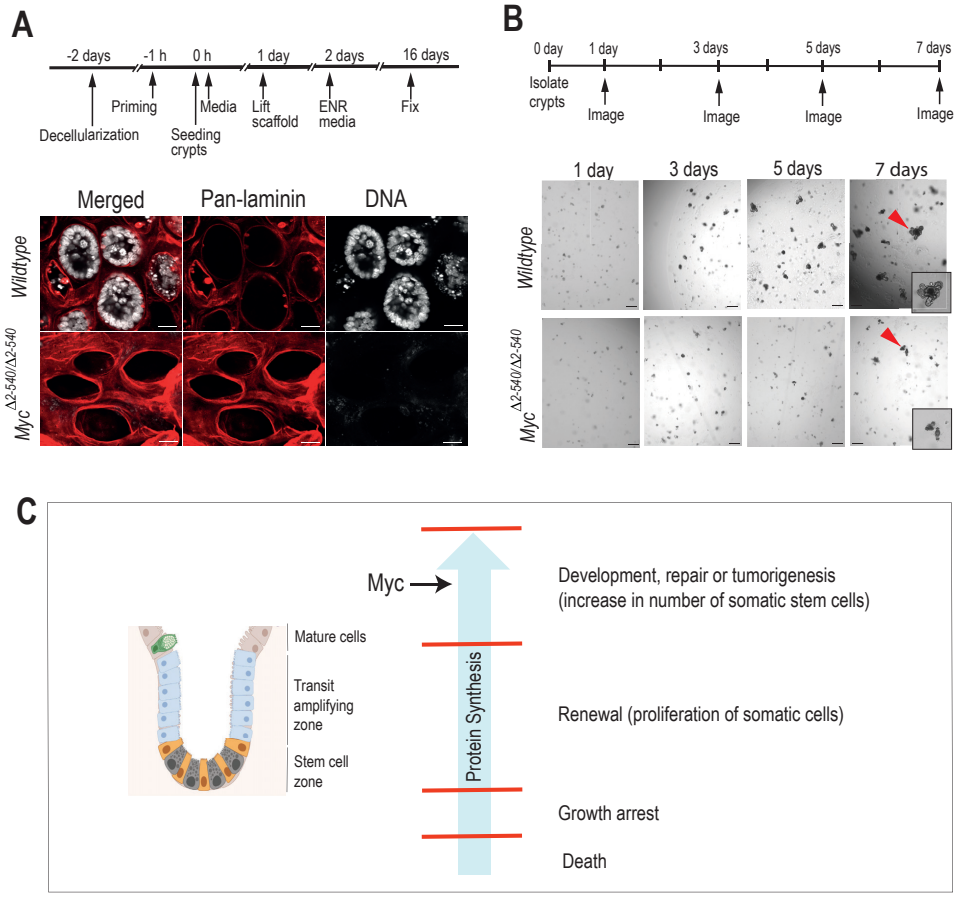

Fig. 4. Myc$^{\Delta 2\text{-}540/\Delta 2\text{-}540}$ intestine fails to support regenerative growth *in vitro* 3-D cultures (a) Immunofluorescence analysis showing failure of Myc$^{\Delta 2\text{-}540/\Delta 2\text{-}540}$ crypts to re-epithelialize intestinal scaffolds. (b) The inability to re-epithelialize the scaffolds is correlated with the inability of crypts from adult Myc$^{\Delta 2\text{-}540/\Delta 2\text{-}540}$ intestine to support organoid growth in culture. (c) Model describing how different levels of protein synthesis can result in different proliferative cell fate choices ranging from normal homeostasis to regeneration and cancer.

Materials and Methods

Animals

Mouse lines used in this study have been described previously (*1, 2*). All mice were on a C57BL/6 genetic background and kept on a 12:12 h light cycle in standard housing conditions and provided with food and water *ad libitum*. Animal experiments were done in accordance with the regulations and with approval of the local ethical committee (Stockholms djurförsöksetiska nämnd). Mice were irradiated with Gammacell® 40 Exactor that uses Caesium-137 as a source for γ-rays. Mice were given 2 doses of 6 Gy with a 6 hr interval in between the doses. After irradiation mice were provided soft food.

Immunohistochemistry (IHC) and RNA *In Situ* hybridization (ISH)

PFA-fixed and paraffin embedded (FFPE) tissues were sectioned at 5 µm thickness and subjected to IHC using standard methods. For antigen retrieval, the sections were boiled in microwave for 20 minutes in 10 mM Citrate buffer pH 6.0 and subsequently processed for respective antibody stainings. Following antibodies and working dilutions were used: anti-Ki67 (Abcam, 1:200), anti-Lysozyme (Abcam, 1:500), anti-Muc2 (Abcam, 1:500), anti-Chga (Abcam, 1:1000). ISH was also performed on 5 µm thick sections using the RNAscope technology and according to manufacturer's protocol. Probes against mouse Myc (catalog nr: 413451) and Lgr5 (catalog nr:312171) were used. RNA integrity was confirmed using the control probe for Ubc (catalog nr:310771) (fig. S3).

qPCR

Approximately 1 cm of distal ileum of mice was cut into small pieces and stored in RNAlater (Thermo Fisher). RNA was prepared using a combination of Trizol (Ambion) and RNeasy mini kit (Qiagen). cDNA was synthesized from 1 µg of total RNA using High Capacity cDNA Reverse Transcription Kit (Applied Biosystems). qPCR was performed using SYBR™ Green master mix (Thermo Fisher) on a LightCycler® 480 instrument (Roche). Primers for *Myc* and *Actin* were as described previously (*2*).

Single-cell RNA-seq (scRNA-seq)

Single cell suspensions of crypt-enriched fractions isolated from mouse small intestine were run on a 10x Chromium controller using the Chromium Next GEM Single Cell 3´kit v3.1 (catalog nr: PN-1000268) and according to manufacturer's protocol (10x Genomics). Cell number targeted was 6000. Briefly intestinal crypts were isolated according to Sato and Clevers (*3*). Crypts were dissociated with TrypLE express (Invitrogen) at 37° for 20 mins to get single cell suspensions. For non-irradiated samples, crypts were isolated from ileum and single cell suspension of FACS sorted $7AAD^{-}$ (Life Technologies), $CD45^{-}$ (eBioscience), $CD31^{-}$ (eBioscience), TER-119^{-} (eBioscience), $EpCAM^{+}$ (eBioscience) cells were used. For irradiated samples, crypts from the whole small intestine were isolated and $7AAD^{-}$ FACS sorted cells were used. Libraries were sequenced on illumina sequencing platform NovaSeq 6000 or NextSeq 2000. Sequencing data was processed using Cell Ranger (v6.0.1) (10x Genomics). Quality control (QC) analysis of the Cell Ranger output was done in Scanpy (v1.9.1) (*4*) as follows: Mean and Standard deviation (SD) of genes in all cells [Mean (n_{genes}), SD(n_{genes})] and Mean, Median, Median absolute deviation (MAD) and SD of total counts in all cells was calculated. Cells were kept with the number of expressed genes larger than [Median(n_{genes})-MAD(n_{genes})], total read counts in the range of [Mean(n_{counts})-1.5*MAD(n_{counts}), Mean(n_{counts})+3*SD(n_{counts}) and percentage of expressed mitochondrial genes larger than its median+3*MAD. Additionally, genes expressed in less than 0.1% of cells were filtered out. Subsequently for dimensional reduction, top 2000 highly variable genes were selected based on the single-cell RNA raw read count matrix (scanpy.pp.highly_variable_genes; flavor= 'seurat_v3'). There were no mitochondrial genes in the top 2000 highly variable genes. The raw read count matrix with top 2000 highly variable genes (22,108 x 2,000) was subjected to the Bayesian variational inference model scVI (v0.16.4) (*5*) to infer a latent space for all single cells. The batch effect among different samples was automatically removed for all samples within the scVI. After that, two-dimensional visualizations were calculated by using Uniform Manifold Approximation and Projection (UMAP). Clustering analysis was performed using Leiden algorithm. First a k-nearest-neighbor graph from the scVI latent space was constructed and then sc.tl.leiden function in scanpy was used with the resolution of 1. This resulted in 19 clusters. The small cluster expressing immunocyte markers (excluded 34 cells and 22,074 cells were kept) was not used for further analysis. Remaining clusters were annotated into 7 intestinal cell types based on previously published marker genes (*6*).

For further analysis, the single cell raw read count matrix of all the genes was input into R package Scran (v1.24.1) to calculate the size factor for each cell (*7*). To normalize the gene expression across cells, each gene's read count in a cell was divided by that cell's size factor in Scanpy. The normalized gene read counts were $\log_2$ transformed, where 1 pseudo count was added to gene's read count to avoid negative infinity value in the analysis (log1p value). The z-score for the log1p value for each gene was calculated and used for heatmap visualization of cell-type specific marker genes.

Differentially expressed genes between the genotypes were determined using scanpy's function sc.tl.rank_genes_groups. The analysis was done specifically in the stem cell (SC), transit amplifying cell (TA) and enterocyte clusters (EC). Within this function, Wilcoxon test was used to calculate p values and the false discovery rate (FDR) by applying the benjamini-hochberg approach. The log fold changes of the 126 known Myc targets (*8*) were retrieved from the differential gene expression results and plotted using a dot plot. Polr1f was not detected in our dataset and was excluded from analysis (table S1). The ranking of the genes on the X-axis was based on the median log fold change values of each Myc target gene among stem cell (SC), transit amplifying cell (TA) and enterocyte (EC) clusters combined.

Gene Set Enrichment Analysis was done using R package clusterProfiler (v4.4.4). Gene signatures were obtained from Gene Ontology Biological Process gene sets (*9*) and the MSigDB 'Hallmark gene sets' (*10*). All the expressed genes in the SC cluster were pre-ranked by their log fold changes which were determined as described in the previous section. GSEA analysis was then performed using ClusterProfiler (ClusterProfiler::GSEA; pvalueCutoff=1, pAdjustMethod=´BH´). The full list of GSEA results is provided in the supplementary table S2.

Single cell ATAC-seq (scATAC-seq)

scATAC-seq was performed according to Cheng *et al 2021* (*11*). Single cell suspensions of mouse intestinal crypts were prepared as in (*12*) and single cells were FACS sorted into 384 well plate with 3 µl lysis buffer in each well (0.03 µl 1M Tris-pH7.4, 0.0078 µl 5M NaCl, 0.075 µl 10% IGEPAL, 0.075 µl RNases Inhibitor, 0.075 µl 1:1.2M ERCC, 2.7372 µl H_2O). After cell lysis, 1µl of the lysis buffer containing the nuclei was used for scATAC library preparation, while the remaining 2 µl were discarded. The scATAC *in situ* tagmentation was performed with 2µl of the Tn5 tagmentation mix (0.06 µl 1M Tris-pH 8.0, 0.0405 µl 1M $MgCl_2$, 0.2 µl Tn5) at 37°C for 30

mins. After tagmentation, 2 µl of the supernatant was aspirated and the nucleus was then washed once with 10 µl ice-cold washing buffer (0.1 µl 1M Tris-pH7.4, 0.02 µl 5M NaCl, 0.03µl 1M $MgCl_2$, 9.85 µl H_2O). The remaining Tn5 was inactivated by adding 2 µl 0.2% SDS-Triton X-100 and incubating at room temperature for 15 mins followed by 55°C for 10 mins. Before barcoding PCR, genomic DNA was extracted from chromatin by adding 2µl Proteinase K (0.0107 au/mL) and incubation at 55°C for 1h followed by heat inactivation at 70°C for 15 mins. Barcoding PCR was done using KAPA HiFi PCR Kit (Roche) in a final volume of 25 µl. The PCR condition was 72°C/15 min, 95°C/45 s, [98°C/15 s, 67°C/30 s, 72°C/1 min] x 22 cycles, 72°C/5 min, and then 4°C hold. After the PCR, 2µl reaction from each well was pooled and cleaned-up twice using SPRI-beads (at 1.3X volume) and the library was sequenced on Illumina NextSeq 550 as paired-end, dual index (37+37+8+8). For scATAC-seq data, raw sequence reads were trimmed based on quality (phred-scaled value of >20) and the presence of illumina adapters, and then aligned to the mm10 genome build using BWA (*13*). Reads that were not mapped, not with primary alignment, missing a mate, mapq <10, or overlapping ENCODEs blacklist regions (*14*) were removed. A custom script was used to summarize the paired-end reads into a de-duplicated fragment file suitable for downstream analysis. scATAC-seq data was analyzed using ArchR. Cells with fewer than 1000 ATAC-seq reads mapping to transcription start site, or with TSS enrichment < 4, were excluded from analysis. The "iterative LSI" function with maxClusters=6 was used for cluster analysis. Clusters with high expression of 'Muc2' were annotated as goblet cells and discarded. Clusters high in 'Ascl2' and 'Lgr5' were annotated as stem cells, while remaining intermediate/low expressing clusters were annotated as Transit amplifying cells. Each of these superclusters were split by genotype and merged to in-silico bulk experiments.

Intestinal crypt isolation and Organoid culture

Crypts were isolated from adult mouse small intestine (approx. 3 month old) according to Sato and Clevers 2013 (*3*). The crypts were seeded in Matrigel (Corning) and cultured in ENR medium (Advanced DMEM/F12 (Thermo Fisher Scientific), 1x penicillin/streptomycin, (Thermo Fisher Scientific), 1x Glutamax (Thermo Fisher Scientific), 10mM HEPES (Thermo Fisher Scientific), 1x B27 and 1x N2 (Thermo Fisher Scientific), 1.25mM N-acetylcysteine (Sigma), 50 ng/ml of murine recombinant Epidermal growth factor (R&D), 100 ng/ml recombinant murine Noggin (R&D), 1 µg/ml recombinant murine R-Spondin (R&D).

Re-epithelialization of intestinal scaffolds with crypts

The ileum from the small intestine of mice, was decellularized as previously described by Iqbal *et al* 2021 (*15*). Pieces of decellularized intestines (dECMs) were primed at 37˚C with 50 µl of media containing Advanced DMEM/F12, 1x penicillin/streptomycin, 1x Glutamax (Thermo Fisher Scientific), 10mM HEPES (Thermo Fisher Scientific), 1x B27 (Life Technologies), 1x N2 (Life Technologies), 1mM N-acetylcysteine (Sigma), 50 ng/ml of murine recombinant Epidermal growth factor (R&D), 100 ng/ml recombinant murine Noggin (Peprotech), 500 ng/ml recombinant murine R-Spondin (R&D), 10µM Y-27632 (Sigma), for 15-60 mins. This was followed by aspirating media carefully and plating around 100 crypts on each scaffold piece and incubating at 37˚C for 10 min. Next, 10 µl of media was added to each scaffold piece and incubated at 37˚C for 10 min, followed by an additional 20 µl per scaffold piece and incubation at 37˚C for 20 min. Finally, 260 µl of media was added to each scaffold piece and put in the incubator at 37˚C. The day after seeding, media was changed, and each scaffold piece was lifted to make it float. The second day after seeding, the media was changed to media without Y-27632. Media was subsequently replaced every other day. Re-epithelialized dECMs were fixed with 4% PFA at day 16 after plating. The re-epithelialized dECMs were analyzed using immunofluorescence. Primary antibody Pan-laminin (1:300, Abcam, 11575) and secondary antibody Alexa-647 conjugated anti-rabbit (1:1000, Life) were used. For nuclei detection, DAPI (Life, 1:1000) was used. Images were obtained with a Zeiss LSM980- Airy2 microscope using a 20x objective, NA=08.